Engineering a Plant Polyketide Synthase for the Biosynthesis of Methylated Flavonoids

Peng, Bo; Zhang, Lili; He, Siqi; Oerlemans, Rick; Quax, Wim J.; Groves, Matthew R.; Haslinger, Kristina

Published in:
Journal of Agricultural and Food Chemistry

DOI:
10.1021/acs.jafc.3c06785

Publication date:
2024

JOURNAL OF AGRICULTURAL AND FOOD CHEMISTRY

pubs.acs.org/JAFC
Article

Engineering a Plant Polyketide Synthase for the Biosynthesis of Methylated Flavonoids

Bo Peng, Lili Zhang, Siqi He, Rick Oerlemans, Wim J. Quax, Matthew R. Groves, and Kristina Haslinger*

Cite This: J. Agric. Food Chem. 2024, 72, 529−539
Read Online

ABSTRACT: Homoeriodictyol and hesperetin are naturally occurring O-methylated flavonoids with many health-promoting properties. They are produced in plants in low abundance and as complex mixtures of similar compounds that are difficult to separate. Synthetic biology offers the opportunity to produce various flavonoids in a targeted, bottom-up approach in engineered microbes with high product titers. However, the production of O-methylated flavonoids is currently still highly inefficient. In this study, we investigated and engineered a combination of enzymes that had previously been shown to support homoeriodictyol and hesperetin production in *Escherichia coli* from fed O-methylated hydroxycinnamic acids. We determined the crystal structures of the enzyme catalyzing the first committed step of the pathway, chalcone synthase from *Hordeum vulgare*, in three ligand-bound states. Based on these structures and a multiple sequence alignment with other chalcone synthases, we constructed mutant variants and assessed their performance in *E. coli* toward producing methylated flavonoids. With our best mutant variant, HvCHS (Q232P, D234 V), we were able to produce homoeriodictyol and hesperetin at 2 times and 10 times higher titers than reported previously. Our findings will facilitate further engineering of this enzyme toward higher production of methylated flavonoids.

KEYWORDS: *site-directed mutagenesis, crystal structure, homoeriodictyol, hesperetin, chalcone synthase, Escherichia coli*

1. INTRODUCTION

Flavonoids are natural polyphenolic compounds ubiquitously found in various flowers, fruits, and vegetables.[1] In nature, flavonoids are important for plant growth and reproduction, for attracting pollinators, and for protecting against biotic and abiotic stresses, such as harmful ultraviolet radiation.[2] More than 15,000 compounds have been identified to date, and many have been shown to have health-promoting effects, such as anticancer, anti-inflammatory, antimutagenic, and antioxidant properties.[3] These health-promoting effects make flavonoids an attractive ingredient for nutraceutical, pharmaceutical, and cosmetic applications.[1]

Homoeriodictyol and hesperetin are important, naturally occurring O-methylated flavonoids, which exhibit higher biological activities and better pharmacological properties, including metabolic stability, membrane transport capability, and oral bioavailability, compared to unmethylated flavonoids.[4] Homoeriodictyol, which is O-methylated in the 3′-position, was previously isolated from *Viscum articulatum* Burm and has been shown to have anticancer effects in MCF-7, HeLa, and HT-29 cells.[5] Furthermore, it was shown to protect endothelial cells from oxidative stress and mitochondrial dysfunction.[6] Hesperetin, which is O-methylated in the 4′-position, has been reported to ameliorate Alzheimer's disease[7] and inhibit the migration of breast cancer.[8] More importantly, hesperetin displays strong inhibitory activity toward several viruses, such as influenza A 14 virus, parainfluenza virus type-3, and SARS-CoV.[9,10]

The current industrial production of flavonoids mainly relies on extraction from plants. This strategy has the limitations that the flavonoid content and yield are variable between seasons and that flavonoids exist in complex mixtures that need to be separated with large volumes of organic solvents. The chemical synthesis of flavonoids requires harsh reaction conditions and toxic substrates which are not eco-friendly.[11]

Another promising route for generating flavonoids is the biosynthesis of flavonoids in microbial cell factories. The rapid development of synthetic biology has enabled the heterologous expression of the flavonoid biosynthesis pathway in microorganisms such as *Escherichia coli* and *Saccharomyces cerevisiae*.[12−15] In the first step, *p*-coumaric acid is activated by 4-coumarate:coenzyme A (CoA) ligase (4CL) to give coumaroyl-CoA (Figure 1). Then, chalcone synthase (CHS) condenses one coumaroyl-CoA and three malonyl-CoA to form naringenin chalcone, which is subsequently converted to the (2S)-naringenin by chalcone isomerase (CHI). In plants, naringenin can be converted to other flavonoids by tailoring enzymes and is thus a key intermediate in the pathway. CHS is the first committed enzyme in flavonoid synthesis and belongs to the superfamily of type three polyketide synthases.[16] Recently many unmethylated flavonoids were directly produced *via* this simple pathway in microbial cell factories by precursor feeding and pathway engineering. For instance, Dunstan *et al.* established high titers for naringenin (484 mg/L from *p*-coumaric acid) and eriodictyol (55 mg/L from caffeic

Received: September 20, 2023
Revised: November 30, 2023
Accepted: December 6, 2023
Published: December 18, 2023

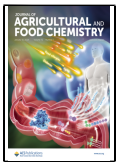

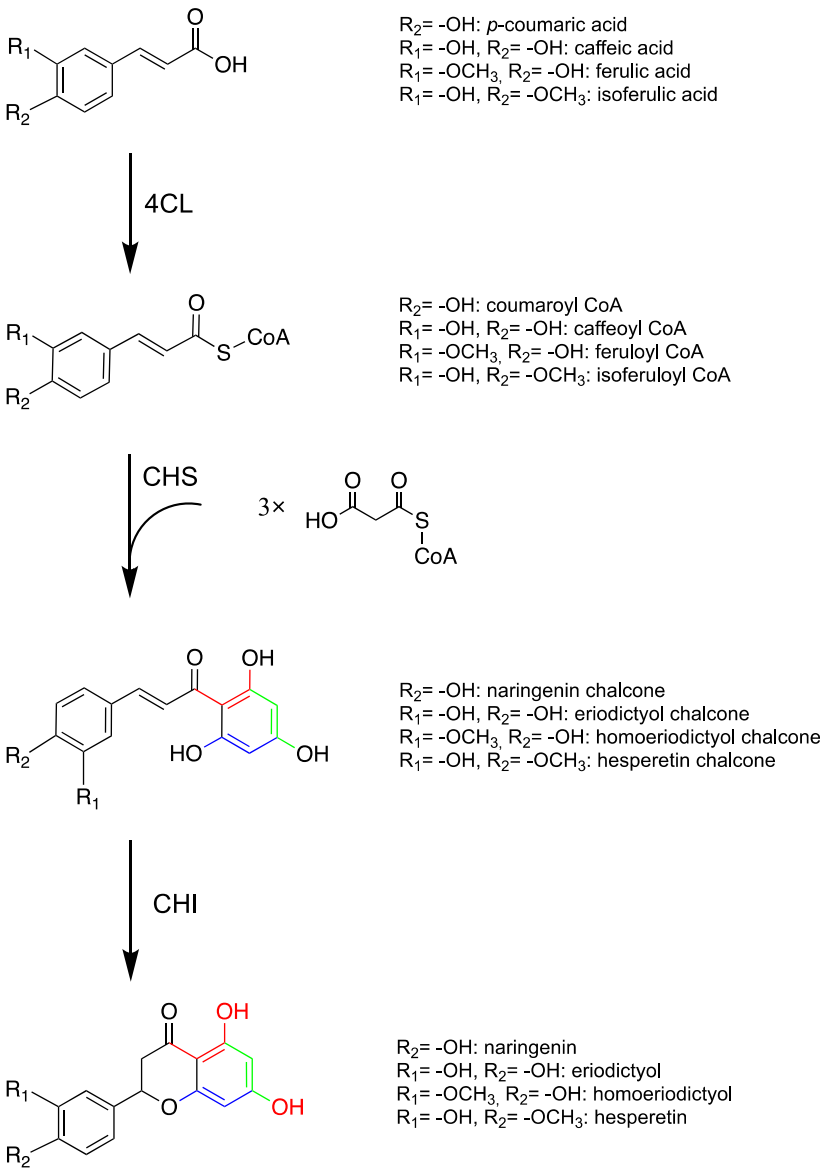

Figure 1. Biosynthesis pathway of the four flavonoids discussed in the study. The natural pathway product in plants is naringenin that is converted into other flavonoids by tailoring enzymes. In this study, eriodictyol, homoeriodictyol, and hesperetin are directly produced by feeding the respective precursors (4CL, 4-coumarate:CoA ligase; CHS, chalcone synthase; CHI, chalcone isomerase).

acid) with a semiautomated metabolic engineering strategy in *E. coli*.[13] Hwang *et al.* developed a systematic strategy for the multilevel optimization of naringenin biosynthetic pathways.[17] The best strain obtained with this approach exhibited a 3-fold increase in naringenin production compared to the parental strain, which was around 260 mg/L naringenin in a fed-batch bioreactor.[17]

Methylated flavonoids such as homoeriodictyol and hesperetin can be obtained by direct methylation of unmethylated flavonoids. For example, Liu *et al.* developed a two-strain system to convert naringenin to hesperetin in resting cells with 66.8% conversion (37.1 mg/L hesperetin).[18] They also leveraged the promiscuous plant flavonoid 3′-hydroxylase and an engineered 4′-*O*-methyltransferase (OMT) for hesperetin *de novo* production in *E. coli* with the highest titer of 27.5 mg/L.[19] Hanko *et al.* combined a previously optimized eriodictyol production pathway with an engineered plant OMT with improved regiospecificity and produced up to 14.6 mg/L hesperetin and 3.8 mg/L homoeriodictyol from 3 mM caffeic acid in *E. coli*.[20] Lastly, Kunzendorf *et al.* recently engineered a bacterial OMT for the regiospecific methylation of eriodictyol dihydrochalcone to hesperidin dihydrochalcone and eriodictyol to hesperetin *in vitro*, with 99:1 and 98:2 regioisomeric ratios, respectively.[21] All of these strategies depend on the preassembled flavonoid scaffold that is either extracted from plant material or built *de novo* in a microbial cell factory. This scaffold is then modified with plant cytochrome P450 enzymes and OMTs. Cytochromes P450 are often regarded as pathway bottlenecks dramatically restricting pathway efficiency.[22] Both enzymes suffer from low regioselectivity and require the supplementation of costly cofactors, NAD(P)H[22] and S-adenosyl methionine,[19,20] respectively.

Another approach is to establish a biosynthetic pathway commencing with simple methylated hydroxycinnamic acids such as ferulic acid and isoferulic acid. These methylated hydroxycinnamic acids are highly abundant in lignocellulosic biomass, can be easily extracted under mild conditions,[23,24] and could therefore be very cost-effective building blocks. This

https://doi.org/10.1021/acs.jafc.3c06785
J. Agric. Food Chem. 2024, 72, 529−539

precursor-directed biosynthesis strategy builds on the ability of the 4CL and CHS enzymes to accept alternative phenolic substrates. 4CL enzymes are known to be quite tolerant toward substitutions of their substrates,[25,26] and for CHS enzymes it has been reported that altering certain residues in the active site improves their enzymatic activity and expands their substrate scope toward non-natural phenolic starter units.[27,28] Recently, Cui *et al.* obtained low final titers of hesperetin (0.4 mg/L) from simple methylated hydroxycinnamic acids by constructing a recombinant *E. coli* strain that expresses 4CL from *Oryza sativa* (Os4CL) and CHS from *Hordeum vulgare* (HvCHS).[29] Since efficient uptake of ferulic acid by *E. coli* has been demonstrated in other studies,[30,31] it is most likely that the low hesperetin titer in this study is related to overall poor enzymatic activity of this enzyme combination, or the fact that ferulic acid and isoferulic acid are poor substrates for these enzymes.

In this study, we set out to explore this enzyme combination further.[32] We determined the crystal structure of HvCHS in complex with CoA, CoA and naringenin, and CoA and eriodictyol. Based on these structures, we designed mutant variants to increase the titers of O-methylated flavonoids homoeriodictyol and hesperetin produced in *E. coli* from fed ferulic acid and iso-ferulic acid.

2. MATERIALS AND METHODS

2.1. Bacterial Strains, Primers, and Plasmids. All of the bacterial strains and plasmids used in this study are listed in Tables S1 and S2. Primers are given in Table S3. *E. coli* DH5a (New England Biolabs) was used for routine cloning and pathway propagation, *E. coli* MG1655 K-12 (DE3)[33] was used for protein expression and fermentation, and *E. coli* BL21 (DE3) was used for protein expression. The genes for PhCHS, CHS from *Petunia hybrida*; MsCHI, CHI from *Medicago sativa*; Pc4CL, 4-CL from *Petroselinum crispum*; HvCHS, CHS from *H. vulgare*; and Os4CL, 4-CL from *O. sativa* were codon-optimized and synthesized from Integrated DNA Technologies with the restriction site introduced (Integrated DNA Technologies, Coralville, Iowa, USA). The genes for PhCHS and HvCHS were cloned between SacI and *Hin*dIII of pETDuet-1 and those for Pc4CL and Os4CL were cloned between NdeI and XhoI of pETDuet-1, yielding pETDuet-PhCHS-Pc4CL and pETDuet-HvCHS-Os4CL, respectively. The gene for MsCHI was cloned between NdeI and XhoI of pCDFDuet-1 and pETDuet-HvCHS, yielding pCDFDuet-MsCHI and pETDuet-HvCHS-MsCHI, respectively. The gene for Os4CL was cloned between NdeI and XhoI of pCDFDuet-1, yielding pCDFDuet-Os4CL. The gene for HvCHS was cloned between ScaI and *Hin*dIII of pET28a, yielding pET28a-HvCHS. The gene for Os4CL was cloned between NdeI and XhoI of pET28a, yielding pET28a-Os4CL. Mutagenesis libraries were generated using QuikChange. All plasmids were isolated with the QIAprep Spin Miniprep kit and were sequence verified.

2.2. Construction of Recombinant *E. coli* Strains. To generate the flavonoid producing *E. coli* strains s1−s20, the respective plasmid combinations were cotransformed into *E. coli* MG1655 (DE3) electrocompetent cells. The protocol for the preparation of electrocompetent *E. coli* was from Green and Sambrook.[34] After transformation, the cells were grown on selective Luria-Bertani (LB) agar (ampicillin and spectinomycin at 100 μg/mL) at 30 °C overnight. The next day, colonies were inoculated in 3 mL of selective LB liquid medium in round-bottom polystyrene tubes for cultivation at 30 °C and 200 rpm overnight. The following day, glycerol stocks were prepared from these cultures (50% (v/v) glycerol) and stored at −80 °C until further usage.

2.3. Multiple Sequence Alignment. Protein sequences were aligned with Clustal Omega (1.2.4) with default settings.[35] The alignment was visualized with AliView.[36] Active site residues of CHS were identified based on Protein Data Bank (PDB) entry 1CGK and those of 4CL based on 5BSW.

2.4. Fermentation Conditions. For small-scale fermentations, the flavonoid pathway expressing strains were streaked in duplicates from glycerol stocks into LB agar plates with ampicillin and spectinomycin (100 μg/mL each). After incubating overnight at 30 °C, single colonies were inoculated into a starter culture of 3 mL of selective LB medium in round-bottom polystyrene tubes and grown with shaking at 200 rpm at 30 °C overnight. The next day, the cultures were diluted 1:100 into 3 mL seed cultures of modified 4-morpholinepropanesulfonic acid (MOPS) medium[15] for 24 h at 30 °C. These were used to inoculate working cultures of 1 mL at an optical density λ = 600 nm (OD_{600}) of 0.05 in a 48 flower-shaped well plate (m2p-labs, Germany) and incubated at 30 °C, 900 rpm in an Eppendorf Thermomixer. Isopropyl-β-D-1-thiogalactopyranoside (IPTG) (final concentration, 1 mM), precursors (final concentration, 1 mM), and cerulenin (final concentration, 20 μg/mL) were added into the cell culture after 6 h, and the incubation was continued for 32 h.

For fermentations in shake flasks, two single colonies of the respective strains were inoculated into starter cultures, as described above. The next day, 1 mL of the starter culture was inoculated into 50 mL of a fresh LB medium. IPTG (final concentration, 1 mM) was added to the culture broths when the OD_{600} reached 0.4−0.6 for protein expression and the cultures were successively incubated at 30 °C for an additional 3 h. The cells were collected by centrifugation for 30 min at 3,100*g* (Eppendorf 5920R, Germany) and 4 °C and then resuspended in 25 mL of fresh modified MOPS medium[15] which included 1 mM precursor, 1 mM IPTG, and 20 μg/mL cerulenin for further 32 h of fermentation.

Samples were taken for the quantification of OD_{600} and extracellular metabolites after 32 h of fermentation. Metabolites were prepared for HPLC and HPLC−MS analysis, as described in Dunstan *et al.*[13] Samples were stored at −20 °C until analysis. OD_{600} was measured by an absorbance plate reader (BMG Labtech, Germany) at 600 nm.

2.5. Analysis and Quantification of Target Compounds. The authentic standards for *p*-coumaric acid, caffeic acid, ferulic acid, isoferulic acid, naringenin, eriodictyol, homoeriodictyol, and hesperetin were purchased from Sigma-Aldrich (USA). The compounds used in *in vitro* experiments (coenzyme A hydrate, malonyl coenzyme A tetralithium salt, and adenosine 5′-triphosphate (ATP) disodium salt hydrate) were purchased from Sigma-Aldrich (USA). The fatty acid synthase inhibitor cerulenin was purchased from Enzo Life Sciences (USA).

Samples from fermentation and *in vitro* turnover were analyzed by HPLC, with a Shimadzu LC-10AT system equipped with an SPD-20A photodiode array detector (PDA). The samples were analyzed by 10 μL injections and separation over an Agilent Eclipse XDB-C18 (5 μm, 4.6 × 150 mm) column with a concentration gradient (solution A: water +0.1% trifluoroacetic acid (TFA), solution B: acetonitrile +0.1% TFA) at a flow rate of 1 mL/min. The following gradient was used: 15% solution B for 3 min, 15−90% solution B over 6 min; 90% solution B for 2 min; 90−15% solution B over 3 min, 15% solution B for 4 min. *p*-Coumaric acid, caffeic acid, ferulic acid, isoferulic acid, naringenin, eriodictyol, homoeriodictyol, and hesperetin were identified by comparison to authentic standards. The peak areas were integrated and converted to concentrations based on calibration curves with the authentic standards (Figure S1).

The identity of hesperetin was furthermore confirmed by HPLC coupled mass spectrometry (HPLC-MS) with a Waters Acquity Arc UHPLC-MS equipped with a 2998 PDA, and a QDa single-quadrupole mass detector (Figure S2). The samples were separated over an XBridge BEH C18 3.5 μm column with a concentration gradient (solution A, water +0.1% formic acid; solution B, acetonitrile +0.1% formic acid) at a flow rate of 0.25 mL/min (1 μL injections). The following gradient was used: 5% solution B for 2 min, 5−90% solution B over 3 min; 90% solution B for 2 min; and 5% solution B for 3 min.

https://doi.org/10.1021/acs.jafc.3c06785
J. Agric. Food Chem. 2024, 72, 529−539

2.6. Protein Expression, Purification, and Crystallization. *2.6.1. Expression.* *E. coli* BL21(DE3) harboring the plasmids pET28a::HvCHS, pET28a::HvCHS(Q232P, D234V), or pET28a::Os4CL were inoculated in 3 mL LB (containing 100 μg mL^{-1} kanamycin) for overnight cultivation at 37 °C and 200 rpm. The next day, 1 mL of overnight cell culture was used to inoculate 1 L of fresh self-induction medium for further 20 h of cultivation at 30 °C and 200 rpm in 5 L glass Erlenmeyer flask. The self-induction medium composition (1 L) consisted of 20 g tryptone, 5 g yeast, 5 g sodium chloride, 4.45 g disodium hydrogen phosphate dihydrate, 3.4 g potassium dihydrogen phosphate, 6 g glycerol, 0.5 g glucose, 1.28 g lactose, and 100 μg mL^{-1} kanamycin.

2.6.2. Purification. All steps were performed with cooled buffers at 4 °C. Cells were harvested by centrifugation at 3,100*g* for 20 min. The cell pellet was resuspended in 20 mL of lysis buffer (50 mM Tris−HCl and 300 mM NaCl, pH 7.6). The cells were disrupted by sonication for 4 × 40 s (with a 5 min rest interval between each cycle) at 60 W output. The unbroken cells and debris were removed by centrifugation (10,000*g* for 1 h). The supernatant was filtered through a syringe filter (pore diameter, 0.45 μm) and incubated with 3 mL of Ni^{2+}-sepharose resin, which had previously been equilibrated with lysis buffer, in a small column at 4 °C for 18 h with agitation. The unbound proteins were eluted from the column using a gravity flow. The column was first washed with lysis buffer (15 mL) and then with buffer A (30 mL, 50 mM Tris−HCl, 300 mM NaCl, and 30 mM imidazole, pH 7.6). Retained proteins were eluted with buffer B (5 mL, 50 mM Tris−HCl, 300 mM NaCl, and 500 mM imidazole, pH 7.6). Fractions were analyzed by separation using sodium dodecyl sulfate polyacrylamide gel electrophoresis (4−12% polyacrylamide) and staining with the InstantBlue Coomassie Protein stain (Abcam, UK). Fractions containing chalcone synthase were pooled and loaded onto a HiLoad 16/600 Superdex 200 pg column, which had previously been equilibrated with buffer C (180 mL, 10 mM HEPES, 50 mM NaCl buffer, 5% glycerol, and 2 mM DTT, pH 8.5). Elution was performed by running buffer C across the column at 1 mL min^{-1} for 1.2 column volumes. Fractions were collected and analyzed by sodium dodecyl sulfate polyacrylamide gel electrophoresis. The purified enzyme was concentrated with centrifugal devices with Omega membrane 30K (Pall, USA) and stored at −80 °C until further use.

2.6.3. Crystallization. Freshly prepared HvCHS was used in crystallization. The protein was concentrated to 10 mg/mL in a buffer consisting of 10 mM HEPES pH 7.5, 50 mM NaCl, 5% (v/v) glycerol, and 2 mM DTT. Screening for crystallization conditions was executed manually using commercial sparse-matrix screening kits (JCSG Plus; PACT premier; Morpheus and the PGA screen; Molecular Dimensions Ltd.), by sitting drop vapor diffusion at 4 °C. After 1−2 days, small crystals were obtained in a drop containing 1 μL protein and 1 μL crystallization buffer (0.1 M MES/imidazole pH 6.5, 0.03 M $MgCl_2$, 0.03 M $CaCl_2$, 20% (v/v) glycerol, and 10% (v/v) PEG4000). The crystallization buffer was optimized to a lower concentration of precipitants (16% (v/v) glycerol and 8% (v/v) PEG4000) to get fewer and larger crystals (Figure S3).

Crystals were harvested 3−4 days before diffraction using a nylon loop. Before flash-cooling in liquid nitrogen, crystals were quickly dipped into a cryoprotectant composed of the reservoir buffer with an increased concentration of glycerol (32% (v/v)).

Some crystals were soaked in a cryoprotectant containing either an additional 1 mM naringenin or 5 mM eriodictyol for 24 h in order to obtain crystals of the enzyme−product complex. Naringenin and eriodictyol were initially prepared as 1 M stock in 100% DMSO.

2.6.3.1. Data Collection, Structure Determination, and Refinement. All diffraction data of HvCHS crystals were collected on beamlines P11 and P13 (operated by EMBL Hamburg) of Petra III at DESY (Hamburg, Germany).[37,38]

Integration, space group determination, and scaling were carried out with XDSAPP[39] and Aimless in the CCP4 suite.[40] The structure of HvCHS complexed with CoA was determined by molecular replacement with the monomer of chalcone synthase from *Arabidopsis thaliana* (PDB: 6DXB) using the program Phaser.[41] Molecular replacement with the DIMPLE pipeline[40] was performed to determine and initially refine the structures of HvCHS in complex with naringenin and eriodictyol, utilizing the polypeptide chain of the HvCHS structure as a starting model.

All structures were iteratively refined using manual adjustment in Coot[42] and Refmac5.[43]

2.6.3.2. PDB Deposition. The structures of HvCHS in complex with CoA, CoA and naringenin, and CoA and eriodictyol were deposited in the PDB under accession codes 8B32, 8B35, and 8B3C, respectively.

2.6.4. Structure Comparison and Visualization. The HvCHS structures were compared to known CHS structures in the PDB and pairwise to each other with the Dali server.[44] Final structures were visualized with PyMOL (Schrödinger, LLC).

2.7. *In Vitro* Synthesis of Feruloyl-CoA. Feruloyl-CoA was synthesized in a 5 mL *in vitro* reaction with purified Os4CL enzyme following established protocols.[25] The reaction mixture [purified enzyme (40 μg/mL), ferulic acid (400 μM), coenzyme A (800 μM), ATP (2.5 mM), and $MgCl_2$ (5 mM) in potassium phosphate buffer (50 mM, pH 7.4)] was incubated at 30 °C in the dark, with mixing at 200 rpm overnight. The reaction product was analyzed by HPLC, then aliquoted, and stored at −20 °C for further experiments.

2.8. *In Vitro* Enzymatic Assay. The *in vitro* enzymatic assays with HvCHS were performed in 50 μL reaction mixtures composed of feruloyl-CoA (2.5, 5, 10, 25, 50, or 100 μM), malonyl-CoA (300 μM), and HvCHS variant (50 nM) in 100 mM phosphate buffer (pH 7.4). The individual reactions were started by adding the enzyme, incubated at 37 °C without mixing, and quenched at different time points (2.5, 5, and 7.5 min) by adding an equal volume of methanol with 0.1% formic acid to quench the reaction. The samples were centrifuged at 10,000*g* for 10 min, and the supernatant was used for HPLC analysis. The integrated peak areas of the product were converted into concentrations based on a calibration curve with the authentic standard and plotted against time (Figure S4). Apparent initial velocities were determined by linear regression over the early time points before 10% substrate conversion was reached. The apparent initial velocities of the biological triplicates were then plotted against the substrate concentrations, and the resulting curves were fitted with the Michaelis−Menten equation in GraphPad prism. Full statistical analysis information is provided in Table S4.

3. RESULTS

Based on the results of previous studies on flavonoid production in *E. coli*, we chose two combinations of CHS and 4CL as a starting point for this study: PhCHS from *P. hybrida* and Pc4CL from *P. crispum*, previously shown to yield high titers of naringenin,[12] and HvCHS from *H. vulgare* and Os4CL from *O. sativa*, previously shown to accept O-methylated hydroxycinnamic acids to form homoeriodictyol and hesperetin.[29] We cloned the genes into coexpression plasmids and transformed them into *E. coli* MG1655 (DE3) (Table S2). In an initial fermentation experiment at 1 mL scale, with fed ferulic acid, and isoferulic acid (1 mM final concentration), we observed that the combination of HvCHS and Os4CL (s2) yielded up to two times higher titers of homoeriodictyol than the other enzyme combination (s1) and that hesperetin was only produced by s2 (Figure S5). Intrigued by this result, we wondered if mutagenesis of the 4CL enzymes to better accommodate the O-methylated substrates could further increase the titers of hesperetin and homoeriodictyol. Based on a previous mutagenesis study showing that the deletion of V341 in the *Nicotiana tabacum* 4CL allows for the binding of double-methylated sinapinic acid,[45] we deleted the corresponding residues in Pc4CL (V342) and Os4CL (V340). Furthermore, based on the crystal structure of the *N. tabacum* 4CL in complex with feruloyl-CoA (PDB: 5BSW),[45] we hypothesized that mutating Q213 and S243 into alanine might

https://doi.org/10.1021/acs.jafc.3c06785
J. Agric. Food Chem. 2024, 72, 529−539

Table 1. Diffraction Data Collection, Structure Determination, and Refinement Statistics[a]

structure name		HvCHS + CoA	HvCHS + CoA, naringenin	HvCHS + CoA, eriodictyol
PDB entry		8B32	8B35	8B3C
space group		$P2_12_12_1$	$P2_12_12_1$	$P2_12_12_1$
unit cell parameter	a, b, c [Å]	a = 77.81	a = 73.91	a = 77.88
		b = 98.96	b = 95.98	b = 97.82
		c = 138.11	c = 138.34	c = 137.93
	α, β, γ [deg]	α = 90.00	α = 90.00	α = 90.00
		β = 90.00	β = 90.00	β = 90.00
		γ = 90.00	γ = 90.00	γ = 90.00
resolution, Å		45.79−1.70 (1.73−1.70)	47.99−2.00 (2.05−2.00)	48.91−2.00 (2.04−2.00)
number of observations		1,556,039 (8,829)	886,223 (8,504)	921,816 (8,357)
completeness, %		99.8 (97.7)	99.9 (99.3)	100 (98.7)
multiplicity		13.2 (13.7)	13.2 (13.5)	12.8 (12.5)
Rmerge		0.07 (1.366)	0.09 (0.476)	0.08 (1.016)
average I/σ,I		18.3 (2.6)	19.8 (6.4)	17.0 (3.1)
CC (1/2)		0.999 (0.885)	0.999 (0.979)	0.999 (0.947)
		Refinement Statistics		
no. reflections, all/free		117,356/5,895	67,037/3,335	71,816/3,554
Rfactor		0.177	0.159	0.198
Rfree		0.205	0.193	0.234
no. of protein atoms		5,859	5,804	5,838
no. of ligand atoms		96	136	138
no. of water atoms		401	367	164
		Average B-Factors, Å^2		
protein		34.58	30.26	50.26
ligands		55.21	56.41	83.47
water		40.78	36.32	48.50
		rmsd from Ideal Values		
bond lengths, Å		0.0129	0.0119	0.0094
bond angles, °		1.757	1.658	1.503
		Ramachandran Plot		
favored, %		96.97	96.31	97.11
allowed, %		2.50	3.03	2.63

[a]Values in brackets refer to the highest resolution shell.

provide more space in the substrate-binding pocket to accommodate the O-methyl group. In Pc4CL, residue 243 is already an alanine. We generated single-point variants of the two 4CL enzymes and screened them in the recombinant flavonoid pathway against the two methylated substrates (Figure S6A,B). We observed a 1.5-fold increase in homoeriodictyol titer with s6 (Os4CL (delV340)) compared to s2, yet the other strains produced equal or lower titers than the wild type (Figure S6A,B). We also generated a double and a triple mutant for Pc4CL and Os4CL, respectively, but did not observe a positive effect on titers (Figure S6C).

Thus, we proceeded with investigating the role of CHS in substrate selection by determining the crystal structures of HvCHS with the ligands CoA, naringenin, and eriodictyol by X-ray crystallography and site-directed mutagenesis.

3.1. Crystal Structure of Chalcone Synthase from *H. vulgare*. The initial crystallization experiments with purified HvCHS yielded high-quality crystals that diffracted to 1.7 Å (Table 1). We solved the phase problem with molecular replacement using PDB: 6DXB[46] without the ligand. The refined structure (PDB: 8B32) shows high structural similarity with several CHS structures in the PDB based on a Dali search[44] (Table S5). The highest Z-scores were determined for CHS1 from *O. sativa*, CHS from *Freesia hybrida*, mutant variants of CHS from *M. sativa* (MsCHS) with various ligands, and CHS1 from *Glycine max* (L.). These enzymes all share an amino acid sequence identity of more than 70% and adopt the typical CHS fold with the $\alpha\beta\alpha\beta\alpha$ pseudosymmetric thiolase motif in the C-terminal domain and the α-helical motif in the N-terminal domain[47] (Figure 2A). In the refined structure, we observed an additional electron density in the substrate-binding cleft separating the N- and C-terminal domains, which we interpreted as CoA. The putative CoA molecule occupies the area of the enzyme previously identified as the malonyl-CoA-binding pocket,[47] and our interpretation of the electron density agrees well with the model of the ligand in the CoA-bound structure of MsCHS (PDB: 1BQ6) (Figure 2B).

To gain further insight into the binding pocket of the hydroxycinnamic acid starter unit, we soaked the crystals of HvCHS with naringenin, eriodictyol, homoeriodictyol, and hesperetin. While soaking with the O-methylated flavonoids impaired crystal diffraction, we were able to determine the structures of the naringenin- (PDB: 8B35) and eriodictyol-bound enzyme (PDB: 8B3C) at 2 Å resolution. In both structures, the electron densities for CoA and the products are well defined, and the position of the bound products agrees well with the MsCHS structure (PDB: 1CGK). All three HvCHS structures are highly congruent, even in residues lining the active site. The only difference can be seen in the β-sheet and loop from L269 to D272 (Figure 2C). Based on the electron density map, this loop appears to adopt two distinct conformations in all three crystal structures. However, while in

https://doi.org/10.1021/acs.jafc.3c06785
J. Agric. Food Chem. 2024, 72, 529−539

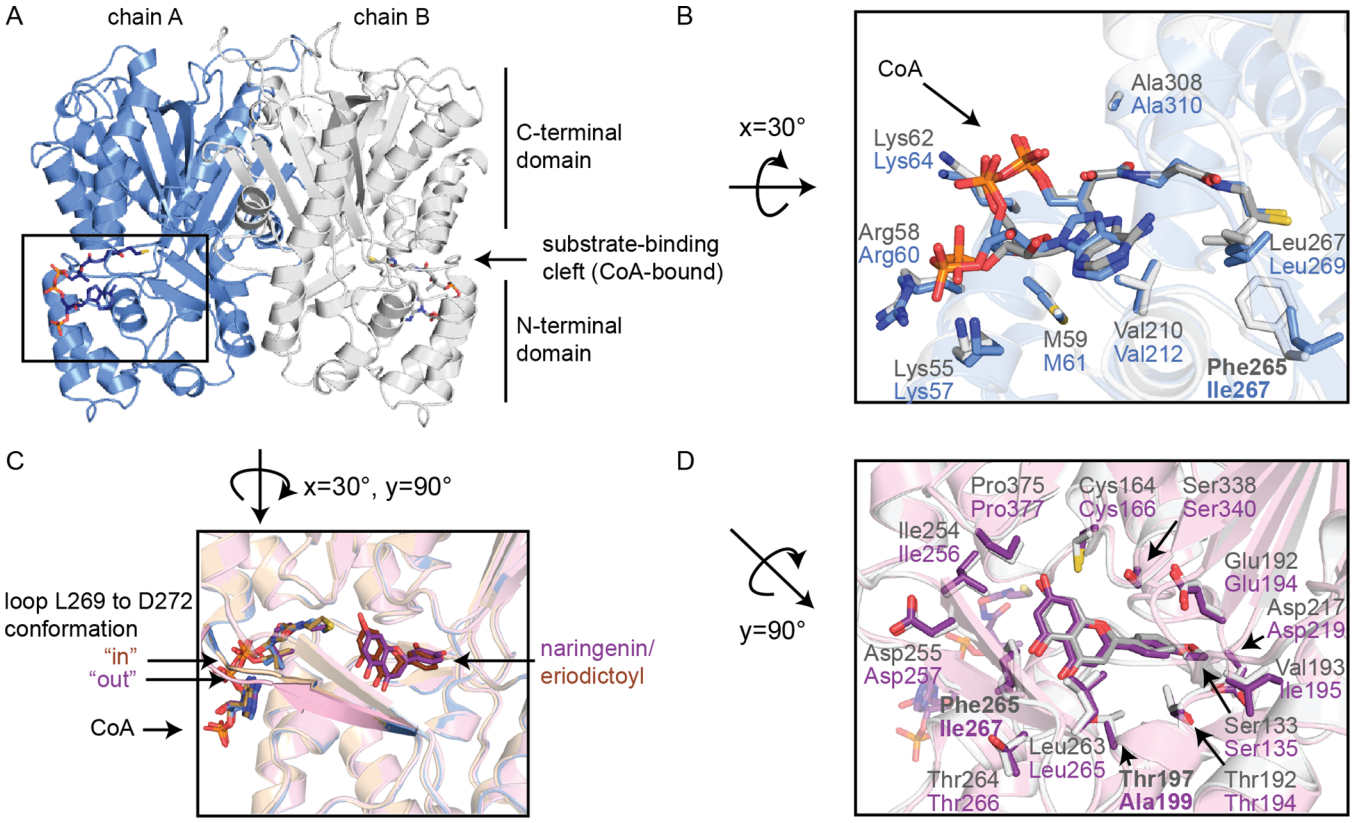

Figure 2. Crystal structures of HvCHS. (A) Overview of the HvCHS fold with the two monomers shown in gray and blue. (B) CoA-binding pocket of HvCHS in complex with CoA (blue) compared to the structure of MsCHS in complex with CoA (PDB: 1BQ6, gray). (C) Overlay of all HvCHS structures (CoA-bound (blue), naringenin-bound (pink), and eriodictoyl-bound (yellow)). (D) Product-binding pocket in HvCHS with naringenin bound (pink) compared to the structure of MsCHS in complex with naringenin (PDB: 1CGK, gray). Atom coloring in ligand representation: oxygen = red, nitrogen = blue, phosphorus = orange, and carbon = color matches the cartoon color of the corresponding structure.

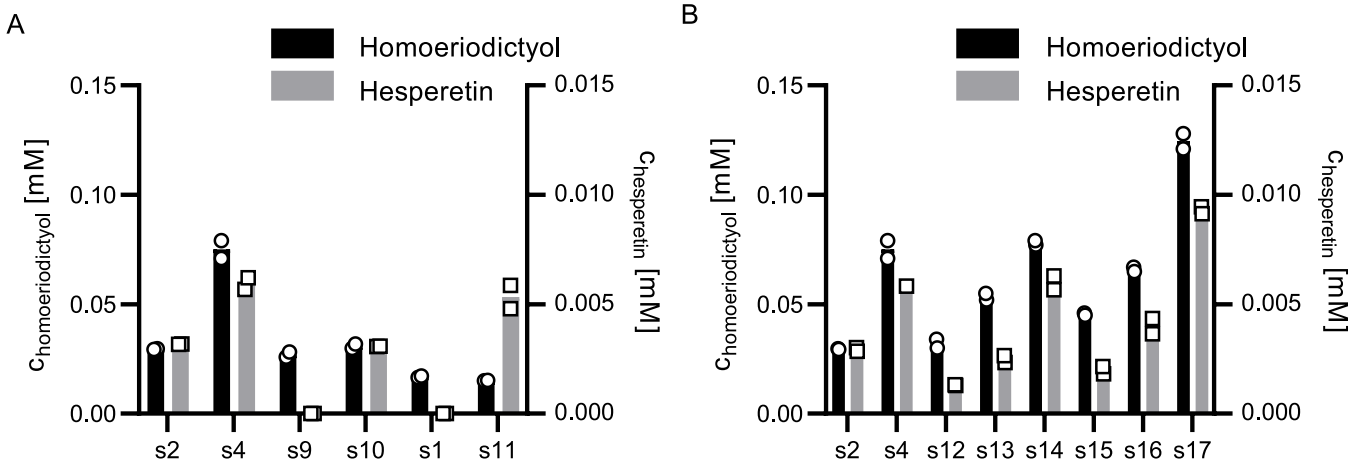

Figure 3. Small-scale fermentation of *E. coli* flavonoid-producing strains expressing CHS variants. Titers of homoeriodictyol (black, left axis) and hesperetin (gray, right axis) were determined 32 h postinduction of enzyme expression and addition of the precursors (1 mM ferulic acid or isoferulic acid). The experiment was performed in duplicate. (A) Comparison of *E. coli* flavonoid-producing strains expressing CHS variants: s1 PhCHS wild type, s11 PhCHS (T197A), s2 HvCHS wild type, s4 loop variant, s9 HvCHS (A199T), and s10 HvCHS (I267F). (B) Comparison of *E. coli* flavonoid-producing strains expressing HvCHS variants: s2 wild type, s4 loop variant, s12-s16 single-point mutation variants, and s17 double-point mutation variant.

the CoA-bound and the CoA/eriodictoyl-bound structures, the "in"-conformation has much higher occupancy and was therefore chosen for the final model, the "out"-conformation is dominant in the naringenin-bound structure. This agrees well with the conformation of this region in the naringenin-bound structure of MsCHS (1CGK, Figure 2D). This may be related to the slight difference in the angle of the A- and C-rings of naringenin and eriodictyol in the active site. The B-ring and all residues surrounding it show identical conformations in both product-bound structures.

Next, we created a multiple sequence alignment of the structurally most similar proteins in the PDB with HvCHS and

https://doi.org/10.1021/acs.jafc.3c06785
J. Agric. Food Chem. 2024, 72, 529−539

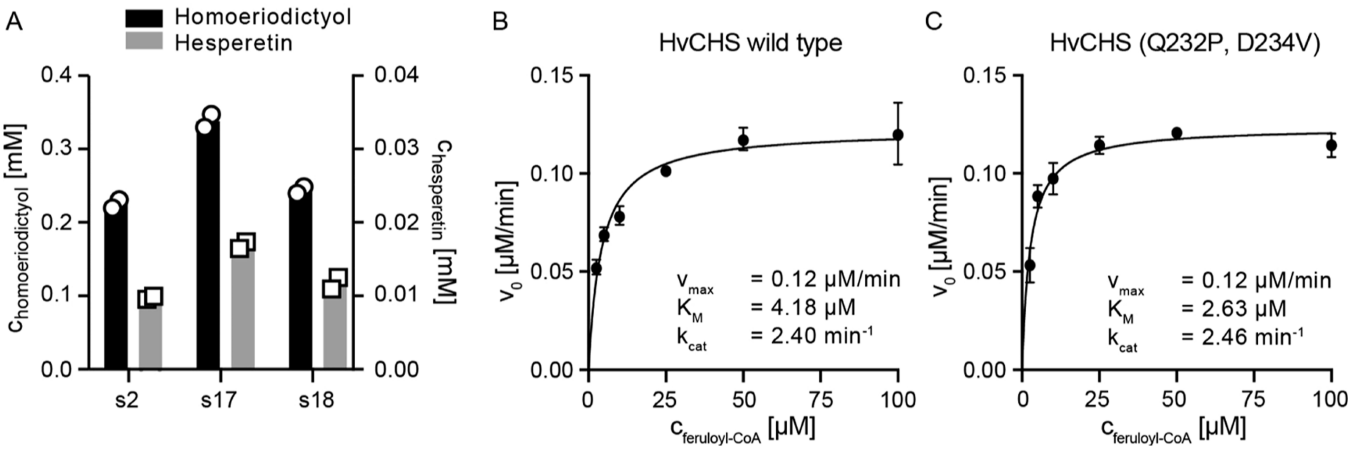

Figure 4. (A) Comparison of HvCHS wild type and double mutant for methylated flavonoid production in shake flask fermentation. Either 1 mM ferulic acid or isoferulic acid was added as a precursor for homoeriodictyol (black, left axis) and hesperetin (gray, right axis), respectively. Samples were taken after 32 h of fermentation and analyzed by HPLC. Each experiment was duplicated. (B,C) Kinetic characterization of HvCHS wild type and HvCHS double mutant for homoeriodictyol formation. Apparent initial velocities were determined at 5, 10, 25, 50, and 100 μM substrate concentration (feruloyl-CoA). Data points represent mean ± SD, n = 3. The full statistical report for nonlinear regression is shown in Table S4.

our other protein of interest PhCHS (Figure S7). When mapping the active site residues known from the well-studied MsCHS enzyme,[47] and our HvCHS structures, it becomes apparent that the residues in the substrate-binding channel and especially the cinnamoyl-binding pocket are highly conserved. The only differences are residue 199 in HvCHS, where the conserved threonine is replaced by an alanine, and residue 267 in HvCHS, where the conserved phenylalanine is replaced by an isoleucine (Figures 2D and S7). Residue 199 is close to the C-ring of naringenin (Figure 2D) and may influence substrate binding, but its importance has not been investigated before. Mutation of the conserved phenylalanine into valine was previously shown to decrease the efficiency of MsCHS by 2-fold, but it did not alter the substrate scope of the enzyme.[47] Further away from the active site, we also noticed a small stretch of amino acids (228−234) with a markedly different sequence in HvCHS compared to those of the other enzymes, although this stretch is not strictly conserved among the other enzymes either. These residues are located on the surface of the enzyme in a loop that follows a β-strand, the opposite end of which forms a part of the active site. Despite the dissimilarity in sequence, this loop adopts the same conformation in the MsCHS and HvCHS crystal structures (Figure S8).

To probe the effect of these minor sequence differences on the enzyme performance for the production of methylated flavonoids *in vivo*, we decided to generate several mutant variants of HvCHS and PhCHS. Our expectation was that certain mutations in HvCHS, *e.g.*, the introduction of the conserved phenylalanine in the active site, could improve its apparent catalytic activity. At the same time, mutations in PhCHS, such as replacing the canonical threonine with an alanine, would enable it to accept O-methylated precursors.

3.2. Screening of CHS Mutant Variants for the Production of Methylated Flavonoids. We constructed PhCHS (T197A), HvCHS (A199T), HvCHS (I267F), and a HvCHS loop variant where the sequence of the surface loop (228−234) is replaced by the sequence of the PhCHS loop. We transformed the resulting plasmids into *E. coli* to generate the flavonoid-producing strains s4, s9, and s10 for the HvCHS variants and s11 for the PhCHS (T197A) variant. We performed small-scale fermentations (1 mL) of these strains feeding 1 mM ferulic acid or isoferulic acid as precursors and sampled 32 h after induction of enzyme expression (Figure 3A). The final optical densities (OD_{600}) of all cultures were similar (ranging from 0.23 to 0.25), suggesting that the mutant variants do not affect the growth or viability of *E. coli*. Both point mutations in HvCHS (s9 and s10) did not alter the final titers of homoeriodictyol compared to s2, yet the A199T mutation completely eliminated hesperetin formation in s9. The analogous point mutation in PhCHS (T197A, s11) for the first time enabled hesperetin production with this enzyme, while the homoeriodictyol titer from this strain is comparable to the strain expressing the wild-type protein (s1). Most interestingly, strain s4 expressing the HvCHS loop variant shows increased titers of both methylated flavonoids with final titers reaching 0.07 and 0.006 mM. These titers are about 2-fold higher than the final titer achieved with HvCHS wild type, and the hesperetin titer is comparable to the one achieved with the PhCHS (T197A) variant (s11). This suggests that the presence of alanine in this position in the active site enables the binding of isoferulic acid, but it does not have a strong effect on ferulic acid binding. Furthermore, the residues in the surface loop also appear to influence the *in vivo* performance of the HvCHS enzyme, yet with an unknown mechanism.

In order to further probe the importance of individual residues of the surface loop for the enhanced *in vivo* performance of the HvCHS loop variant (A228S, D231I, Q232P, L233G, and D234V), we next constructed single mutants for those five sites *via* site-directed mutagenesis. We transformed the resulting plasmids into *E. coli* (s12−s16) and compared the final titers of fermentations with these strains to the ones expressing HvCHS wild type and the loop variant (s2 and s4, respectively). Compared with s4, only s14 and s16 yielded similar or higher product titers (Figure 3B). S12 produced lower and s13 and s15 similar titers as s2 expressing wild-type HvCHS. Therefore, we combined the two best point mutations into a double mutant HvCHS (Q232P and D234V) and transformed the resulting plasmid into *E. coli* (s17). This strain yields higher titers of the methylated flavonoids than all other strains, with final homoeriodictyol titers 2-fold higher

https://doi.org/10.1021/acs.jafc.3c06785
J. Agric. Food Chem. 2024, 72, 529−539

and final hesperetin titers 3-fold higher than that of strain s2 expressing wild-type HvCHS (Figure 3B).

3.3. Further Optimization of Flavonoid Production. To test if we could further increase the titers of methylated flavonoids with our HvCHS variant, we explored a different plasmid configuration. Santos *et al.* emphasized the significance of balancing gene expression levels in enhancing naringenin production.[12] They achieved the highest naringenin titers, when CHS and CHI were expressed from the first and second multiple cloning sites (MCSs) of pETDuet-1, respectively, and 4CL from the first MCS of pCDFduet-1.[12] Thus, we constructed expression plasmids c19 and c20 with our best mutant variant according to this design and cotransformed them into *E. coli* (s18). We performed fermentation at a larger scale in shake flasks to see how the titers for methylated flavonoids from s18 compare to those of s2 and s17 (Figure 4A). We found that the final titers of both products from s18 are comparable to those obtained with s2 (0.24 mM for homoeriodictyol and 0.011 mM for hesperetin). The final titers of homoeriodictyol and hesperetin are the highest with s17, 0.33, and 0.016 mM, respectively. We next examined the production of two unmethylated flavonoids, naringenin and eriodictyol, from their respective hydroxycinnamic acid precursors with our best strain in shake flasks. After 32 h, we achieved titers of 41 and 45 mg/L, respectively. Overall, our best strain s17 produces similar or higher titers of the four flavonoids compared to the study of Cui *et al.*[29]

3.4. Enzymatic Assay for HvCHS Variants. Intrigued by the observation that the surface loop residues of HvCHS have an impact on the enzyme's *in vivo* performance, we endeavored to further examine this phenomenon *in vitro*. We expressed and purified HvCHS wild type and double mutant (Q232P, D234V) with protein yields of 48 and 93 mg protein/L culture, respectively. This suggests that the double mutant has a higher expression level, is more soluble, or is more stable during purification than the wild-type enzyme. Given that homoeriodictyol is the main product *in vivo*, we performed steady-state kinetic assays for wild type and double mutant using feruloyl-CoA as a substrate at a fixed malonyl-CoA concentration. Plotting the apparent initial reaction velocities over the substrate concentration allowed us to fit the data with the Michaelis–Menten equation (Figures 4B,C and S4, Table S4). The apparent kinetic parameters v_{max} and k_{cat} are virtually the same for both HvCHS variants, whereas there is a 1.6-fold difference in the K_M. This indicates that the HvCHS (Q232P, D234V) variant exhibits a higher affinity toward feruloyl-CoA than the wild type and is in good agreement with our results from homoeriodictyol production *in vivo*. In summary, the enhanced biosynthesis of flavonoids (naringenin, eriodictyol, homoeriodictyol, and hesperetin) in *E. coli* expressing the HvCHS double mutant (Q232P, D234V) can likely be attributed to the combined effects of a higher protein expression level and a higher affinity to methylated substrates.

4. DISCUSSION

Hesperetin and homoeriodictyol are valuable natural O-methylated flavonoids that display bioactivity for treating human diseases. Recently, Cui *et al.* obtained hesperetin and homoeriodictyol at a low titer through precursor-directed biosynthesis in engineered *E. coli* from fed isoferulic acid and ferulic acid.[29] The enzymes used in that study had previously been shown to have high substrate promiscuity *in vitro*[26,48] and were then used *in vivo* for the first time.[29] To become industrially relevant, the yield and productivity of such a pathway must be dramatically increased, and enzymes must be highly selective for the O-methylated substrates to allow for the use of low-cost substrates. Thus, to facilitate further enzyme engineering efforts, we determined the crystal structures of one of the enzymes of this pathway, HvCHS, in complex with its products and analyzed a multiple sequence alignment with the most similar structures in the PDB. Since all CHS enzymes are highly conserved overall, especially in the substrate-binding pockets, we did not see any obvious reasons why HvCHS would accept O-methylated precursors and other CHS enzymes would not. However, we identified three areas of interest for rational enzyme engineering—two amino acids in the substrate-binding pocket that are markedly different from the consensus sequence (A199 and I267 in HvCHS) and a surface-exposed loop that is connected to the active site through a β-strand and has more polar residues than in the other CHS sequences. Indeed, mutating the conserved Thr at position 197 in PhCHS enabled this enzyme to produce hesperetin for the first time. However, replacing I267 with the canonical Phe did not alter the performance of HvCHS. Surprisingly, mutating two of the polar or charged residues of the surface loop into hydrophobic amino acids increased the final titers of methylated flavonoids *in vivo*. We were able to show that this is likely attributable to a boost in protein abundance and an increase in affinity for methylated hydroxycinnamic acid.

The final titers that we achieved for both methylated flavonoids in a larger-scale experiment exceed the titers previously reported by Cui *et al.*[29] by 2- and 10-fold for homoeriodictyol and hesperetin production, respectively. These titers are now in the same order of magnitude as those of other biosynthetic approaches that introduce the O-methylations as late-stage modifications.[18−20] Compared to homoeriodictyol, hesperetin production is still very low, mainly due to the substrate preference of HvCHS. In the future, this substrate preference can be further shifted by directed evolution or rational engineering based on our crystal structure. In particular, in light of our surprising findings about the surface loop distant from the active site, it is worth exploring other positions in the multiple sequence alignment that are markedly different in HvCHS compared to other CHS enzymes. Alternatively, as more than 1000 putative plant CHSs have now been predicted *via* computational tools, it is also interesting to investigate the substrate scope and catalytic activity of these new enzymes to possibly replace the workhorse CHS enzymes with ones that are better suited for the large-scale production of hesperetin and other flavonoids. Lately, researchers have also identified noncanonical CHSs (NRPS-PKS) and the biosynthetic pathway for flavonoids in fungi.[49,50] Exploring the substrate range and catalytic activity of these recently discovered enzymes is intriguing as it could potentially lead to the substitution of the conventional CHS enzymes. This substitution might be advantageous for the efficient production of hesperetin and other flavonoids. Lastly, an alternative strategy could involve employing host strains that possess an ample supply of malonyl-CoA for enhanced flavonoid synthesis.

■ ASSOCIATED CONTENT

Supporting Information

The Supporting Information is available free of charge at https://pubs.acs.org/doi/10.1021/acs.jafc.3c06785.

https://doi.org/10.1021/acs.jafc.3c06785
J. Agric. Food Chem. 2024, 72, 529−539

Gene and primer sequences, list of plasmids and strains, results of Dali analysis, statistical analysis of steady-state kinetics, calibration curves for product quantification by HPLC, HPLC−MS identification of fermentation products, micrograph of protein crystals, time progress curves for steady-state kinetics, product titers of fermentations with strains s1, s2, s3, s5-s8, s19, and s20 expressing 4CL variants, sequence comparison of CHS enzymes, and illustration of HvCHS surface loop (PDF)

AUTHOR INFORMATION

Corresponding Author

Kristina Haslinger − *Chemical and Pharmaceutical Biology, Groningen Research Institute of Pharmacy, University of Groningen, Groningen 9713AV, The Netherlands;* orcid.org/0000-0003-1361-1508; Email: k.haslinger@rug.nl

Authors

Bo Peng − *Chemical and Pharmaceutical Biology, Groningen Research Institute of Pharmacy, University of Groningen, Groningen 9713AV, The Netherlands*

Lili Zhang − *XB20 Drug Design, Groningen Research Institute of Pharmacy, University of Groningen, Groningen 9713AV, The Netherlands*

Siqi He − *Chemical and Pharmaceutical Biology, Groningen Research Institute of Pharmacy, University of Groningen, Groningen 9713AV, The Netherlands*

Rick Oerlemans − *XB20 Drug Design, Groningen Research Institute of Pharmacy, University of Groningen, Groningen 9713AV, The Netherlands*

Wim J. Quax − *Chemical and Pharmaceutical Biology, Groningen Research Institute of Pharmacy, University of Groningen, Groningen 9713AV, The Netherlands;* orcid.org/0000-0002-5162-9947

Matthew R. Groves − *XB20 Drug Design, Groningen Research Institute of Pharmacy, University of Groningen, Groningen 9713AV, The Netherlands;* orcid.org/0000-0001-9859-5177

Complete contact information is available at: https://pubs.acs.org/10.1021/acs.jafc.3c06785

Author Contributions

K.H. and B.P. conceived the study with contributions from L.Z., S.H., R.O., W.J.Q., and M.G.; B.P. and S.H. cloned plasmids and performed fermentations; B.P. and K.H. analyzed biochemical data; L.Z. and R.O. performed crystallization and diffraction experiments; L.Z., R.O., and M.G. determined and refined the crystal structures; K.H. and B.P. wrote the manuscript with contributions from L.Z., S.H., R.O., W.J.Q., and M.G.; all authors have read and approved the final version of the manuscript.

Funding

B.P., L.Z., and S.H. were supported by promotion scholarships from the Chinese Scholarship Council (202008420246, 202006320070, and 201806300121). K.H. is grateful for funding from the European Union's Horizon 2020 research and innovation program under the Marie Skłodowska-Curie grant agreement no. 893122. W.Q. was supported by SNN, Netherlands 338 (grant number: OPSNN0315).

Notes

The authors declare no competing financial interest.

ACKNOWLEDGMENTS

The authors acknowledge DESY (Hamburg, Germany) and EMBL Hamburg for provision of the PETRA III beamline (P11 and P13). K.H., B.P., S.H., and W.J.Q. thank Serj Koshian for designing the initial set of mutant enzymes during his summer internship, Dr. Robbert Hans Cool for providing training in protein purification, and Nika Sokolova for help with troubleshooting the steady-state kinetics. The submitted version of this manuscript is available on BioRxiv.[32]

ABBREVIATIONS AND NOMENCLATURE

4CL, 4-coumarate:CoA ligase; CHI, chalcone isomerase; CHS, chalcone synthase; CoA, coenzyme A; HPLC, high-performance liquid chromatography; MS, mass spectrometry; TFA, trifluoroacetic acid

REFERENCES

(1) Panche, A. N.; Diwan, A. D.; Chandra, S. R. Flavonoids: An Overview. *J. Nutr Sci.* **2016**, *5*, No. e47.

(2) Samanta, A.; Das Gouranga, D. S. K. Roles of Flavonoids in Plants. *Int. J. Pharm. Sci. Tech* **2011**, *6* (1), 12−35.

(3) Kumar, S.; Pandey, A. K. Chemistry and Biological Activities of Flavonoids: An Overview. *Scientific World Journal* **2013**, *2013*, 1−16.

(4) Koirala, N.; Thuan, N. H.; Ghimire, G. P.; Van Thang, D.; Sohng, J. K. Methylation of Flavonoids: Chemical Structures, Bioactivities, Progress and Perspectives for Biotechnological Production. *Enzyme Microb. Technol.* **2016**, *86*, 103−116.

(5) Saquib, Q.; Ahmed, S.; Ahmad, M. S.; Al-Rehaily, A. J.; Siddiqui, M. A.; Faisal, M.; Ahmad, J.; Alsaleh, A. N.; Alatar, A. A.; Al-Khedhairy, A. A. Anticancer Efficacies of Persicogenin and Homoeriodictyol Isolated from Rhus Retinorrhoea. *Process Biochem.* **2020**, *95* (September 2019), 186−196.

(6) Shen, T.; Li, H.-Z.; Li, A.-L.; Li, Y.-R.; Wang, X.-N.; Ren, D.-M. Homoeriodictyol Protects Human Endothelial Cells against Oxidative Insults through Activation of Nrf2 and Inhibition of Mitochondrial Dysfunction. *Vasc. Pharmacol.* **2018**, *109* (December 2017), 72−82.

(7) Kheradmand, E.; Hajizadeh Moghaddam, A.; Zare, M. Neuroprotective Effect of Hesperetin and Nano-Hesperetin on Recognition Memory Impairment and the Elevated Oxygen Stress in Rat Model of Alzheimer's Disease. *Biomed. Pharmacother.* **2018**, *97*, 1096−1101.

(8) Hermawan, A.; Putri, H.; Utomo, R. Y. Comprehensive Bioinformatics Study Reveals Targets and Molecular Mechanism of Hesperetin in Overcoming Breast Cancer Chemoresistance. *Mol. Divers* **2020**, *24* (4), 933−947.

(9) Dong, W.; Wei, X.; Zhang, F.; Hao, J.; Huang, F.; Zhang, C.; Liang, W. A Dual Character of Flavonoids in Influenza A Virus Replication and Spread through Modulating Cell-Autonomous Immunity by MAPK Signaling Pathways. *Sci. Rep.* **2014**, *4* (1), 7237.

(10) Lin, C.-W.; Tsai, F.-J.; Tsai, C.-H.; Lai, C.-C.; Wan, L.; Ho, T.-Y.; Hsieh, C.-C.; Chao, P.-D. L. Anti-SARS Coronavirus 3C-like Protease Effects of Isatis Indigotica Root and Plant-Derived Phenolic Compounds. *Antiviral Res.* **2005**, *68* (1), 36−42.

(11) Marsafari, M.; Samizadeh, H.; Rabiei, B.; Mehrabi, A.; Koffas, M.; Xu, P. Biotechnological Production of Flavonoids: An Update on Plant Metabolic Engineering, Microbial Host Selection and Genetically Encoded Biosensors. *Biotechnol. J.* **2020**, *15*, 1900432.

(12) Santos, C. N. S.; Koffas, M.; Stephanopoulos, G. Optimization of a Heterologous Pathway for the Production of Flavonoids from Glucose. *Metab. Eng.* **2011**, *13* (4), 392−400.

(13) Dunstan, M. S.; Robinson, C. J.; Jervis, A. J.; Yan, C.; Carbonell, P.; Hollywood, K. A.; Currin, A.; Swainston, N.; Le Feuvre, R.; Micklefield, J.; Faulon, J.-L.; Breitling, R.; Turner, N.; Takano, E.; Scrutton, N. S. Engineering Escherichia Coli towards de Novo

Production of Gatekeeper (2S)-Flavanones: Naringenin, Pinocembrin, Eriodictyol and Homoeriodictyol. *Synth Biol.* **2020**, *5* (1), ysaa012.
(14) Koopman, F.; Beekwilder, J.; Crimi, B.; van Houwelingen, A.; Hall, R. D.; Bosch, D.; van Maris, A. J.; Pronk, J. T.; Daran, J.-M. De Novo Production of the Flavonoid Naringenin in Engineered Saccharomyces Cerevisiae. *Microb. Cell Factories* **2012**, *11* (1), 155.
(15) Dinh, C. V.; Prather, K. L. J. Development of an Autonomous and Bifunctional Quorum-Sensing Circuit for Metabolic Flux Control in Engineered Escherichia Coli. *Proc. Natl. Acad. Sci. U.S.A.* **2019**, *116* (51), 25562−25568.
(16) Sun, W.; Meng, X.; Liang, L.; Jiang, W.; Huang, Y.; He, J.; Hu, H.; Almqvist, J.; Gao, X.; Wang, L. Molecular and Biochemical Analysis of Chalcone Synthase from Freesia Hybrida in Flavonoid Biosynthetic Pathway. *PLoS One* **2015**, *10* (3), No. e0119054.
(17) Hwang, H. G.; Noh, M. H.; Koffas, M. A. G.; Jang, S.; Jung, G. Y. Multi-Level Rebalancing of the Naringenin Pathway Using Riboswitch-Guided High-Throughput Screening. *Metab. Eng.* **2021**, *67* (July), 417−427.
(18) Liu, J.; Tian, M.; Wang, Z.; Xiao, F.; Huang, X.; Shan, Y. Production of Hesperetin from Naringenin in an Engineered Escherichia Coli Consortium. *J. Biotechnol.* **2022**, *347*, 67−76.
(19) Liu, J.; Xiao, Z.; Zhang, S.; Wang, Z.; Chen, Y.; Shan, Y. Restricting Promiscuity of Plant Flavonoid 3′-Hydroxylase and 4′- O -Methyltransferase Improves the Biosynthesis of (2 S)-Hesperetin in E. Coli. *J. Agric. Food Chem.* **2023**, *71* (25), 9826−9835.
(20) Hanko, E. K. R.; Correia, J.; Souza, C. S.; Green, A.; Chromy, J.; Stoney, R.; Yan, C.; Takano, E.; Lousa, D.; Soares, C. M.; Breitling, R. Microbial Production of the Plant Flavanone Hesperetin from Caffeic Acid. *BMC Res. Notes* **2023**, *16* (1), 343.
(21) Kunzendorf, A.; Zirpel, B.; Milke, L.; Ley, J. P.; Bornscheuer, U. T. Engineering an O -methyltransferase for the Regioselective Biosynthesis of Hesperetin Dihydrochalcone. *ChemCatChem* **2023**, *15*, No. e202300951.
(22) Urlacher, V. B.; Girhard, M. Cytochrome P450 Monooxygenases in Biotechnology and Synthetic Biology. *Trends Biotechnol.* **2019**, *37* (8), 882−897.
(23) Johnston, P. A.; Zhou, H.; Aui, A.; Wright, M. M.; Wen, Z.; Brown, R. C. A Lignin-First Strategy to Recover Hydroxycinnamic Acids and Improve Cellulosic Ethanol Production from Corn Stover. *Biomass Bioenergy* **2020**, *138*, 105579.
(24) Fu, Y.; Zhang, J.; Guan, T. High-Value Utilization of Corn Straw: From Waste to Wealth. *Sustainability* **2023**, *15* (19), 14618.
(25) Rautengarten, C.; Baidoo, E.; Keasling, J. D.; Scheller, H. V. A Simple Method for Enzymatic Synthesis of Unlabeled and Radiolabeled Hydroxycinnamate-CoA. *Bioenergy Res.* **2010**, *3* (2), 115−122.
(26) Lee, Y.-J.; Jeon, Y.; Lee, J. S.; Kim, B.-G.; Lee, H.; Ahn, J.-H. Enzymatic Synthesis of Phenolic CoAs Using 4-Coumarate:Coenzyme A Ligase (4CL) from Rice. *Bull. Korean Chem. Soc.* **2007**, *28* (3), 365−366.
(27) Bhan, N.; Cress, B. F.; Linhardt, R. J.; Koffas, M. Expanding the Chemical Space of Polyketides through Structure-Guided Mutagenesis of Vitis Vinifera Stilbene Synthase. *Biochimie* **2015**, *115*, 136−143.
(28) Jez, J. M.; Bowman, M. E.; Noel, J. P. Expanding the Biosynthetic Repertoire of Plant Type III Polyketide Synthases by Altering Starter Molecule Specificity. *Proc. Natl. Acad. Sci. U.S.A.* **2002**, *99* (8), 5319−5324.
(29) Cui, H.; Song, M. C.; Lee, J. Y.; Yoon, Y. J. Microbial Production of O-Methylated Flavanones from Methylated Phenylpropanoic Acids in Engineered Escherichia Coli. *J. Ind. Microbiol. Biotechnol.* **2019**, *46* (12), 1707−1713.
(30) Li, B.; He, X.; Zhang, S.; Chang, S.; He, B. Efficient Synthesis of 4-O-*β*-d-Glucopyranosylferulic Acid from Ferulic Acid by Whole Cells Harboring Glycosyltransferase GTBP1. *Biochem. Eng. J.* **2018**, *130*, 99−103.
(31) Yoon, S.-H.; Li, C.; Lee, Y.-M.; Lee, S.-H.; Kim, S.-H.; Choi, M.-S.; Seo, W.-T.; Yang, J.-K.; Kim, J.-Y.; Kim, S.-W. Production of Vanillin from Ferulic Acid Using Recombinant Strains of Escherichia Coli. *Biotechnol. Bioprocess Eng.* **2005**, *10* (4), 378−384.
(32) Peng, B.; Zhang, L.; He, S.; Oerlemans, R.; Quax, W. J.; Groves, M. R.; Haslinger, K. Engineering a Plant Polyketide Synthase for the Biosynthesis of Methylated Flavonoids. *bioRxiv* **2022**, 1−27 preprint.
(33) Nielsen, D. R.; Yoon, S.-H.; Yuan, C. J.; Prather, K. L. J. Metabolic Engineering of Acetoin and Meso-2, 3-Butanediol Biosynthesis in E. Coli. *Biotechnol. J.* **2010**, *5* (3), 274−284.
(34) Green, M. R.; Sambrook, J. Transformation of Escherichia Coli by Electroporation. *Cold Spring Harb Protoc* **2020**, *2020* (6), 101220.
(35) Madeira, F.; Pearce, M.; Tivey, A. R. N.; Basutkar, P.; Lee, J.; Edbali, O.; Madhusoodanan, N.; Kolesnikov, A.; Lopez, R. Search and Sequence Analysis Tools Services from EMBL-EBI in 2022. *Nucleic Acids Res.* **2022**, *50* (W1), W276−W279.
(36) Larsson, A. AliView: A Fast and Lightweight Alignment Viewer and Editor for Large Datasets. *Bioinformatics* **2014**, *30* (22), 3276−3278.
(37) Meents, A.; Reime, B.; Stuebe, N.; Fischer, P.; Warmer, M.; Goeries, D.; Roever, J.; Meyer, J.; Fischer, J.; Burkhardt, A.; Vartiainen, I.; Karvinen, P.; David, C. Development of an In-Vacuum x-Ray Microscope with Cryogenic Sample Cooling for Beamline P11 at PETRA III. *Proceedings of SPIE—the International Society for Optical Engineering TA—TT*; Lai, B., Ed., 2013; Vol. *8851*, p 88510K.
(38) Cianci, M.; Bourenkov, G.; Pompidor, G.; Karpics, I.; Kallio, J.; Bento, I.; Roessle, M.; Cipriani, F.; Fiedler, S.; Schneider, T. R. P13, the EMBL Macromolecular Crystallography Beamline at the Low-Emittance PETRA III Ring for High- and Low-Energy Phasing with Variable Beam Focusing. *J. Synchrotron Radiat.* **2017**, *24* (1), 323−332.
(39) Krug, M.; Weiss, M. S.; Heinemann, U.; Mueller, U. XDSAPP: A Graphical User Interface for the Convenient Processing of Diffraction Data Using XDS. *J. Appl. Crystallogr.* **2012**, *45* (3), 568−572.
(40) Winn, M. D.; Ballard, C. C.; Cowtan, K. D.; Dodson, E. J.; Emsley, P.; Evans, P. R.; Keegan, R. M.; Krissinel, E. B.; Leslie, A. G. W.; McCoy, A.; McNicholas, S. J.; Murshudov, G. N.; Pannu, N. S.; Potterton, E. A.; Powell, H. R.; Read, R. J.; Vagin, A.; Wilson, K. S. Overview of the CCP4 Suite and Current Developments. *Acta Crystallogr. D Biol. Crystallogr.* **2011**, *67* (4), 235−242.
(41) McCoy, A. J.; Grosse-Kunstleve, R. W.; Adams, P. D.; Winn, M. D.; Storoni, L. C.; Read, R. J. Phaser Crystallographic Software. *J. Appl. Crystallogr.* **2007**, *40* (4), 658−674.
(42) Emsley, P.; Lohkamp, B.; Scott, W. G.; Cowtan, K. Features and Development of Coot. *Acta Crystallogr. D Biol. Crystallogr.* **2010**, *66* (4), 486−501.
(43) Murshudov, G. N.; Skubák, P.; Lebedev, A. A.; Pannu, N. S.; Steiner, R. A.; Nicholls, R. A.; Winn, M. D.; Long, F.; Vagin, A. A. REFMAC5 for the Refinement of Macromolecular Crystal Structures. *Acta Crystallogr. D Biol. Crystallogr.* **2011**, *67* (4), 355−367.
(44) Holm, L. Dali Server: Structural Unification of Protein Families. *Nucleic Acids Res.* **2022**, *50* (W1), W210−W215.
(45) Li, Z.; Nair, S. K. K. Structural Basis for Specificity and Flexibility in a Plant 4-Coumarate:CoA Ligase. *Structure* **2015**, *23* (11), 2032−2042.
(46) Liou, G.; Chiang, Y.-C.; Wang, Y.; Weng, J.-K. Mechanistic Basis for the Evolution of Chalcone Synthase Catalytic Cysteine Reactivity in Land Plants. *J. Biol. Chem.* **2018**, *293* (48), 18601−18612.
(47) Noel, J. P.; Ferrer, J. L.; Jez, J. M.; Bowman, M. E.; Dixon, R. A. Structure of Chalcone Synthase and the Molecular Basis of Plant Polyketide Biosynthesis. *Nat. Struct. Biol.* **1999**, *6* (8), 775−784.
(48) Christensen, A. B.; Gregersen, P. L.; Schröder, J.; Collinge, D. B. A Chalcone Synthase with an Unusual Substrate Preference Is Expressed in Barley Leaves in Response to UV Light and Pathogen Attack. *Plant Mol. Biol.* **1998**, *37* (5), 849−857.
(49) Zhang, H.; Li, Z.; Zhou, S.; Li, S. M.; Ran, H.; Song, Z.; Yu, T.; Yin, W. B. A Fungal NRPS-PKS Enzyme Catalyses the Formation of the Flavonoid Naringenin. *Nat. Commun.* **2022**, *13* (1), 6361.

(50) Zhang, W.; Zhang, X.; Feng, D.; Liang, Y.; Wu, Z.; Du, S.; Zhou, Y.; Geng, C.; Men, P.; Fu, C.; Huang, X.; Lu, X. Discovery of a Unique Flavonoid Biosynthesis Mechanism in Fungi by Genome Mining. *Angew. Chem.* **2023**, *62* (12), No. e202215529.

https://doi.org/10.1021/acs.jafc.3c06785
J. Agric. Food Chem. 2024, 72, 529−539